ARTICLE

Large crystalline domains homogenization *via* solvent exchange-coupled dry annealing for ultrastrong and ultratough hydrogels

Ningxin Chen,[1] Jie Deng,[1] Shanchen Yang,[1] Kunkun Guo,[1,*] Sida Xie,[1] Jinwei Song,[1,2] Ji Liu,[3,*] and Zhaohui Wang[1,*]

*Correspondence: sunnywang@hnu.edu.cn (Z. W); kunkunguo@hnu.edu.cn (K. G); liuj9@sustech.edu.cn (J. L)

Received: May 23, 2024; Accepted: October 10, 2024; Published Online: October 16, 2024; https://doi.org/10.59717/j.xinn-mater.2024.100101

GRAPHICAL ABSTRACT

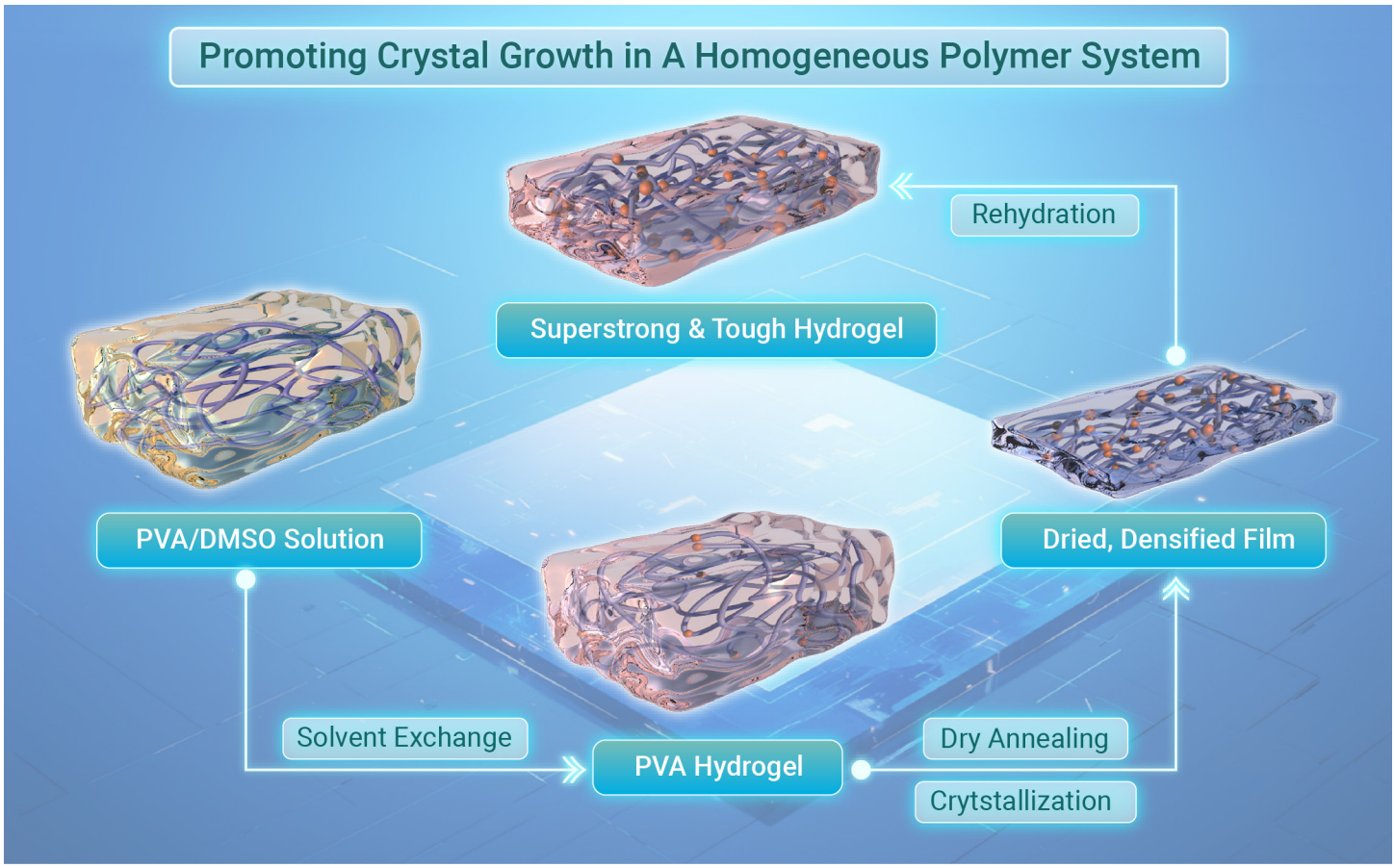

PUBLIC SUMMARY

- An integrated solvent exchange and dry annealing approach to prepare polyvinyl alcohol hydrogels.
- Toughening hydrogel with uniformly distributed, large, and densely crosslinked crystalline domains.
- Achieved an ultrahigh tensile strength of 34.15 MPa and a toughness of 95.21 MJ m^{-3}.

ARTICLE

Large crystalline domains homogenization *via* solvent exchange-coupled dry annealing for ultrastrong and ultratough hydrogels

Ningxin Chen,[1] Jie Deng,[1] Shanchen Yang,[1] Kunkun Guo,[1,*] Sida Xie,[1] Jinwei Song,[1,2] Ji Liu,[3,*] and Zhaohui Wang[1,*]

[1]College of Materials Science and Engineering, Hunan University, Changsha 410082, China

[2]Zhejiang Fulai New Materials Co., Ltd, Jiashan 314100, China

[3]Department of Mechanical and Energy Engineering, Southern University of Science and Technology, Shenzhen 518055, China

*Correspondence: sunnywang@hnu.edu.cn (Z. W); kunkunguo@hnu.edu.cn (K. G); liuj9@sustech.edu.cn (J. L)

Received: May 23, 2024; Accepted: October 10, 2024; Published Online: October 16, 2024; https://doi.org/10.59717/j.xinn-mater.2024.100101

Citation: Chen N., Deng J., Yang S., et al., (2024). Large crystalline domains homogenization *via* solvent exchange-coupled dry annealing for ultrastrong and ultratough hydrogels. The Innovation Materials **2(4)**: 100101.

Current hydrogel fabrication techniques often fall short of simultaneously optimizing key structural parameters, such as network uniformity, crosslinking density, and crystalline domain size, essential for achieving superior mechanical performance. Herein, we introduce a solvent exchange coupled dry-annealing technique, revolutionizing the synthesis of polyvinyl alcohol (PVA) hydrogels. This strategy seamlessly integrates the uniformity afforded by solvent exchange with the benefits of anisotropic densification and crystallization induced by dry annealing, thereby transforming the microstructural configuration of polymer networks, achieving unprecedented uniformity, along with adjustable crystalline domains density and size. Consequently, the resulting PVA hydrogels feature a robust, highly organized network with densely packed, and large crystalline domains. These hydrogels exhibit extraordinary mechanical strength with stress levels reaching 34.15 MPa and toughness (up to 95.21 MJ m^{-3}), supplemented by a fracture energy of 99.2 kJ m^{-2}, significantly outperforming traditional hydrogels. Further enhancement of mechanical properties was achieved through a salting-out process, boosting strength to 52.5 MPa and toughness to 167.9 MJ m^{-3}. This advancement not only ushers in a new era of hydrogel technology but also opens avenues for creating advanced hydrogels with tailored mechanical properties for a variety of sophisticated applications.

INTRODUCTION

Hydrogels, known for their exceptional softness, responsiveness, and biocompatibility, have become indispensable in diverse applications ranging from tissue engineering[1-3] and flexible electronics[4-7] to soft robotics.[8-12] Despite these advancements, the inherent loosely bound network structure of conventional hydrogels often compromises their load-bearing capabilities, thus limiting their practical utility in demanding applications. To address this challenge, extensive research efforts have focused on enhancing the mechanical robustness of hydrogels, through strategies such as transforming polymer microphases into nanofibers[13-15] and constructing double networks.[16,17] However, these approaches have generally fallen short in significantly improving crystallinity, giving rise to hydrogels with stress levels below 5 MPa, indicating only modest mechanical enhancements.

Recent research has highlighted the profound impact of the salting-out[18,19] and wet-annealing[20,21] processes on enhancing hydrogel crystallinity and reducing inter-crystalline distances, leading to improved mechanical properties. Salting-out, effective across various kosmotropic salts and polymer systems, notably improves the stress resilience of hydrogels, including those made from gelatin.[22] This discovery has paved the way for applying salting-out techniques to PVA hydrogels. When combine d with freeze casting, salting-out has produced PVA hydrogels with significant tensile anisotropy,[23] showcasing horizontal strengths ranging from 11.5 MPa to 23.5 MPa. However, this method often compromise the vertical strength of the hydrogels, typically falling below 3 MPa. The application of solvent exchange, in conjunction with salting out,[24] has been shown to create a more uniform PVA polymer network and optimize the distribution of crosslinking points, resulting in isotropic strengths reaching up to 24.7 MPa. However, challenges such as salt diffusion in aqueous environments limit the practical applications of salting out in PVA hydrogel preparation. Furthermore, proposals for annealing hydrogels[25] aim to bolster crystalline domain formation and growth. PVA hydrogels subjected to solvent exchange followed by wet annealing[20] have demonstrated enhanced molecular chain entanglement and crosslinking density. However, the volume of these hydrogels remains largely unchanged post-treatment, indicating a limitation in enhancing network density and, consequently, a maximum mechanical strength of only 11.19 MPa. It is evident that the mechanical attributes of PVA hydrogels are fundamentally influenced by the uniformity and crosslinking density of the polymer network, and crystalline domain size. However, methods that effectively address all these aspects simultaneously are rare, presenting a significant barrier to further improvements in the mechanical properties of PVA hydrogels.

In this study, we introduce a solvent-exchange coupled dry-annealing strategy for fabricating PVA hydrogels that significantly enlarge crystalline domains while ensuring unparalleled uniformity and cross-linking density across the polymer network (Figure 1). We begin by dissolving PVA in dimethyl sulfoxide (DMSO), followed by a water exchange process that replaces traditional, often inhomogeneous, water-based freeze-thaw methods, which leads to the formation of homogenous hydrogel networks. Subsequently, dry annealing above the glass transition temperature meticulously evaporates water,[21] inducing anisotropic drying and controlled shrinkage. This step not only elevates crystallinity but also promotes a densely cross-linked polymer network, in contrast to the volume-conserving wet annealing process. The synergistic effect of solvent exchange and dry annealing culminates in a rehydrated hydrogel characterized by extraordinary crystallinity (46.73%) and an optimized polymer network, leading to extraordinary mechanical properties, including a tensile stress of 34.15 MPa, toughness of 95.21 MJ m^{-3}, and fracture energy of 99.2 kJ m^{-2}, marking a significant leap forward in hydrogel technology. This research not only advances the field of hydrogel preparation but also paves the way for the design and synthesis of multifunctional, high-performance hydrogels. By overcoming the constraints of conventional processes, our novel approach offers promising avenues for the development of hydrogels with tailored properties suitable for a wide range of applications.

MATERIALS AND METHODS

Materials and chemicals: PVA-1799 (98–99% hydrolyzed, Aladdin), DMSO (Aladdin), glycerol (Aladdin), Na_2SO_4 (Aladdin), $ZnSO_4$ (Aladdin), $Al_2(SO_4)_3$ (Aladdin) and Li_2SO_4 (Aladdin).

Preparation of PVA hydrogels: Freeze-thawed (FT) hydrogel, PVA (0.6 g) was dissolved in 4 mL of deionized water, stirred at 90°C for 5 h under a cover to minimize evaporation. The degassed solution was cast in Teflon molds and subjected to freeze-thaw cycles (-12°C for 8 h, thawed at 25°C for 2 h), repeated twice to yield FT hydrogels. FT hydrogels were further annealed at 110°C to form a film, then rehydrated to equilibrium to obtain FTDA hydrogels; solvent exchanged (SE) Hydrogel: 0.6 g PVA was dissolved in 4 mL DMSO and stirred for 5 h at 90°C with coverage to minimize evaporation. After defoaming, the transparent solutions were poured into Teflon molds and then immersed in 200 mL deionized water at room temperature for 24 h to obtain the SE hydrogel. The resultant SE hydrogels were then annealed at varied temperatures (90°C, 110°C, 130°C) and rehydrated to form SEDA hydrogels. Annealing at 110°C was standard unless stated otherwise. For the SEWA hydrogel, following SE hydrogel preparation, molds were immersed in a 200 mL glycerol for 24 h, then annealed at 110°C and rehydrated to yield SEWA hydrogels. Noted that 1 h drying time is optimal for balancing crys-

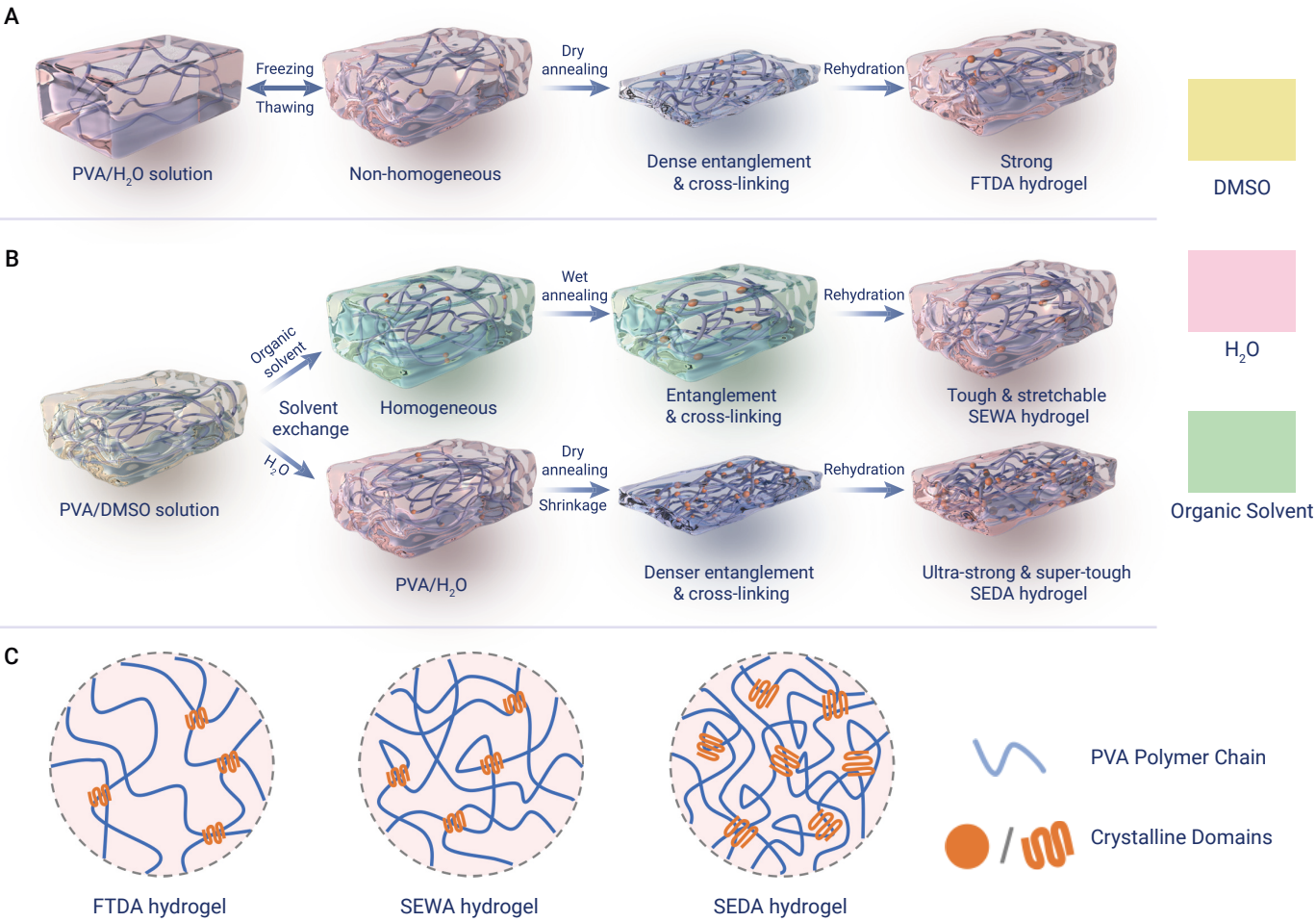

Figure 1. Comparative overview of hydrogel fabrication techniques (A) FTDA hydrogels undergo two freeze-thaw cycles before being subjected to dry annealing and subsequent rehydration. (B) SEWA hydrogels result from solvent exchange from a PVA/DMSO mixture to glycerol, followed by wet annealing and subsequent solvent exchange with water; SEDA hydrogels are formed through direct solvent exchange from PVA/DMSO to water, culminating in dry annealing and rehydration. (C) Macromolecular configurations characteristic of FTDA, SEWA, and SEDA hydrogels, respectively.

tallinity and maintaining hydrogel integrity.

Mechanical measurements: Mechanical tests were conducted using the WDW-01D instrument equipped with a 100 N load cell. Hydrogel samples for tensile tests were prepared with a gauge length of 10 mm and a width of 2 mm. In successive loading-unloading tensile tests, the strain speed was set at 200 mm/min. The young's modulus was determined by analyzing the slope of the initial linear domain of the stress-strain curve. Toughness was calculated as the area under the tensile stress-strain curve. Fracture energy was assessed through pure shear testing. In brief, force-displacement curves were obtained for both notched and unnotched samples with identical initial dimensions and under the same testing conditions. With denoting of the sample cross section area as A, the critical distance where the notch turned into a running crack as *Lc*, and the work done to an unnotched sample to reach *Lc* as U(*Lc*), the fracture energy can be calculated as

$$\Gamma = \frac{U(L_c)}{A}$$

All mechanics data were obtained from at least three independent samples and expressed as the mean ± standard deviation.

Microstructural analysis: Scanning Electron Microscopy (SEM) images were recorded with a TESCAN MIRA3 LM instrument to characterize microscopic structures of hydrogels. Fourier Transform Infrared (FTIR) spectra were obtained on a Nicolet iS 10 spectrometers assisted by ATR attachments. The transmittance of hydrogels was measured at a Shimadzu UV-3600i Plus spectrometer. Atomic Force Microscopy (AFM) phase images were obtained with a Bruker Dimension Icon in tapping mode to visualize crystalline and amorphous regions within the hydrogels.

Water content measurement: The hydrogel samples were dried in an oven at 60°C for 2 days until completely desiccated to determine the water content. The weights of the sample before and after drying were measured as $W_{swollen}$ and W_{dry}, respectively. The water content (W) can be calculated as

$$W = (1 - \frac{W_{dry}}{W_{swollen}}) \times 100\%$$

Crystallinity content measurement: A differential scanning calorimeter (DSC Q20 V24.10 Build 122) was utilized to measure the crystallinity of the PVA hydrogels in their dry state. In a standard Differential scanning calorimetry (DSC) measurement, the total mass of the dry sample was initially weighed. The sample was then placed in a Tzero Pan and heated from 50°C to 250°C at a rate of 20 °C/min. The enthalpy (Hcrystalline) for the melting of crystalline domains per unit mass of the sample can be calculated by integrating the endothermic transition from 200 to 250°C. Therefore, the the crystallinity in the dry sample (X_{dry}) can be calculated as

$$X_{dry} = \frac{H_{crystalline}}{H^0_{crystalline}}$$

where = 138.6 J/g is the enthalpy of the fusion of 100 wt% crystalline PVA measured at the equilibrium melting point. With denoting of the water content of the swollen-state sample as W, the crystallinity in the swollen sample can be calculated as

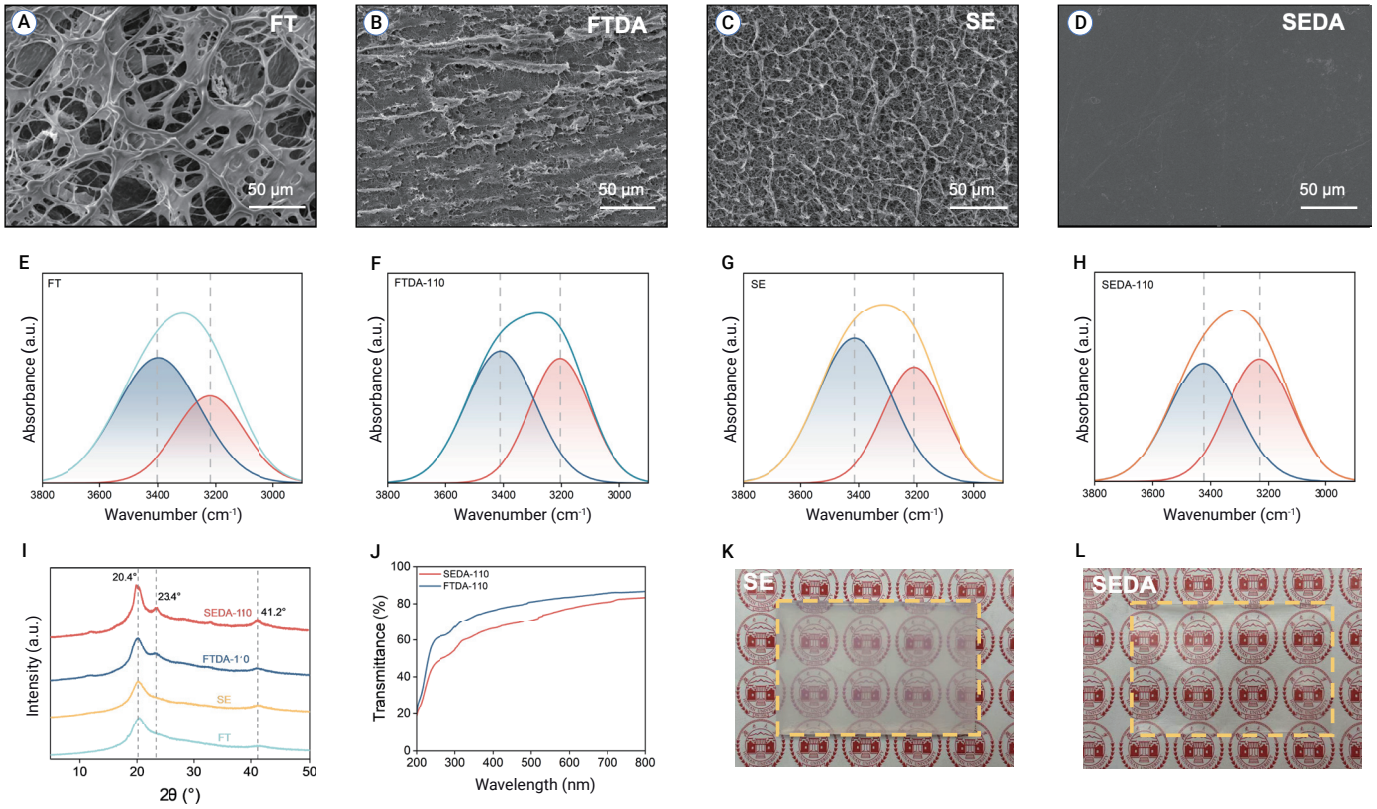

Figure 2. Evolution of hydrogel structures SEM images of (A) FT, (B) FTDA, (C) SE, and (D) SEDA hydrogel. ATR-FTIR spectra of (E) FT, (F) FTDA, (G) SE, and (H) SEDA hydrogel. (I) XRD spectra. (J) Transmittance spectra. (K-L) Optical images of (K) SE and (L) SEDA hydrogel.

$$X_{swollen} = X_{dry}(1 - W)$$

X-ray diffraction (XRD) and Small-Angle X-ray Scattering (SAXS): XRD analysis was performed on a MiniFlex600, with crystalline domain size (D) calculated using Scherrer's equation. SAXS measurements on a Xeuss 2.0 instrument estimated the inter-crystalline domain distance (L) using Bragg's law and fitted using SasView software with a spherical model.

RESULTS AND DISCUSSION

Densified homogeneous polymer network *via* SEDA

To examine the effects of solvent exchange and dry annealing on hydrogel structures, we conducted SEM analyses on hydrogels subjected to freeze-thaw cycles and those treated with solvent exchange. SEM images (Figures 2A & C) revealed that both FT and SE hydrogels exhibit a porous architecture with interconnected filaments. However, FT hydrogels were characterized by large, inconsistently distributed pores, suggesting a less robust polymer network. In contrast, SE hydrogels, formed through direct solvent exchange from PVA/DMSO to water, displayed a more uniform structure with smaller, regularly spaced pores, indicating a more organized arrangement of polymer chains compared to the water-based FT hydrogels. Upon dry annealing at 110°C, the hydrogels underwent noticeable densification. SEM images (Figures 2B, D & S1) showed that the freeze-thaw-assisted dry annealed (FTDA) hydrogels retained some surface irregularities and pore structures, whereas the solvent exchange-coupled dry annealed (SEDA) hydrogels presented a smooth, pore-less surface, reflecting a highly homogeneous and compact polymer network.

FTIR spectroscopy (Figures 2E-H) revealed two smaller peaks at approximately 3210 cm^{-1} and 3405 cm^{-1}, corresponding to hydroxyl group vibrations associated with PVA-PVA and PVA-water interactions, respectively.[26,27] The peak area ratio at 3210 cm^{-1} to the total peak area was calculated for FT, FTDA-110, SE, and SEDA-110 hydrogels (Figure S2), yielding values of 36%, 44%, 40%, and 49%, respectively. This suggests a denser arrangement of polymer chains in hydrogels formed through solvent exchange. Moreover, this trend persists after dry annealing, implying that solvent exchange establishes a compact network of polymer chains within hydrogels while dry annealing further enhances chain mobility, thereby amplifying this advantage.

In Figure 2I, XRD analysis showed that both FT and SE hydrogels initially displayed common diffraction peaks at 20.4° and 41.2°, corresponding to the (101) plane of semi-crystalline PVA and the (102) plane of PVA, respectively. After the post-annealing process, both the FTDA and SEDA hydrogels revealed a new diffraction peak at 23.4°, attributed to the (200) plane of PVA polymer crystals.[28] This indicates a notable increase in crystallinity, suggesting the dry annealing process effectively promote the organization of polymer chains into more defined crystalline structures. Moreover, the intensity of the pre-existing peaks at 20.4° and 41.2° markedly increased in both the FTDA and SEDA hydrogels after annealing. Notably, the peak at 20.4° in the SEDA hydrogels became more pronounced, with a sharper definition and a reduced half-peak width.

DSC was employed to further investigate the crystalline behavior (Figure S3). The enthalpy peaks and crystallinity of SE hydrogel surpassed those of FT hydrogel in both dry and wet states, as observed after dry annealing.[29] Dry annealing greatly enhances the overall crystallinity of hydrogel samples. Additionally, the transparency of SEDA hydrogel was slightly lower at 83.35% compared to 86.74% for the FTDA hydrogel (Figure 2J), which can be attributed to the influence of crystalline domains on light reflection and refraction, further confirming the enhanced crystallinity of SEDA hydrogel. The impact of dry annealing on hydrogel transparency is notably distinct, with SE hydrogels displaying significantly less transparency than their SEDA counterparts, as evident in Figures 2K-L. This variance in transparency can largely be attributed to the reconfiguration of hydrogen bonds within the PVA network during annealing, crosslinking the polymer chains into a more coherent structure that facilitates uniform light transmission and reduces scattering.[30,31]

To further understand the impact of dry annealing on hydrogel microstructure, we analyzed SE hydrogels annealed at different temperatures (SEDA-X, where X represents 90°C, 110°C, and 130°C) through SEM. As shown in

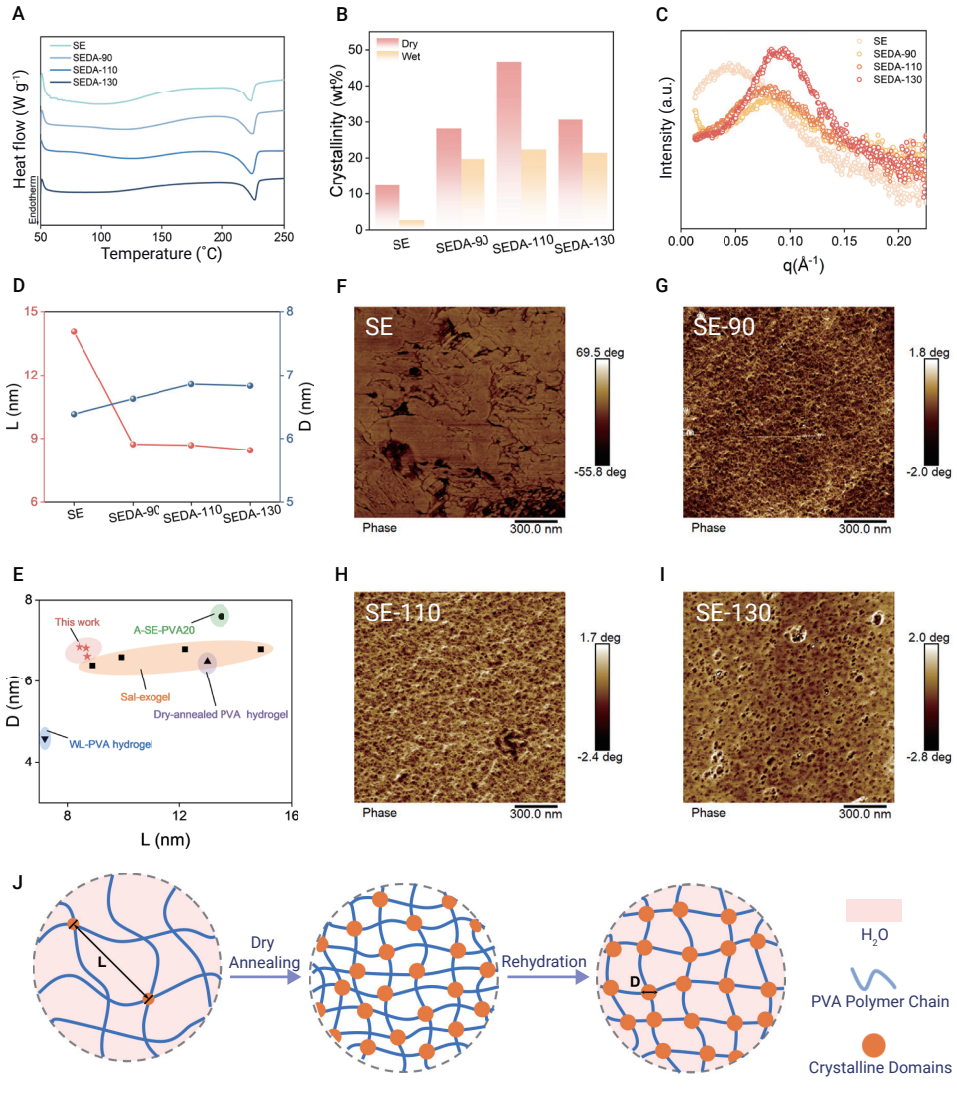

Figure 3. Crystallinity enhancement in hydrogel structural evolution (A) DSC thermograph of the different hydrogels. (B) Calculated crystallinities in dry and swollen states. (C) SAXS profiles of different hydrogels. (D) Average size of the crystalline domains (*D*) and average distance between adjacent crystalline domains (*L*) of different PVA Hydrogels. (E) Comparative analysis of *D* versus *L* for various PVA hydrogels. (F-I) AFM phase images of SE hydrogel (F), SEDA-90 (G), SEDA-110 (H), and SEDA-130 (I), where bright domains correspond to crystalline domains, while dark areas represent amorphous domains. (J) Schematic illustration PVA crystal formation during solvent exchange and dry annealing.

Figure S4, SEDA-90 hydrogels presented a markedly rugged surface with randomly distributed larger pores. Cross-sectional SEM images confirmed that all SEDA hydrogels possess a pore-less, dense polymer network, as shown in Figure S5. Whereas SEDA-130 hydrogels exhibited a highly dense, almost plate-like structure with minimal pore presence. This density in SEDA-130 hydrogels notably hindered water molecule penetration during rehydration, potentially limiting its water content and increasing friction among PVA chains and affecting mechanical properties. Conversely, the SEDA-110 hydrogels demonstrated a balance of surface smoothness and mesopore distribution. The analysis indicated that annealing temperature influences the hydrogel's microstructural, crystalline domains, and potentially its mechanical properties.

Adjustable large crystalline domains *via* SEDA

DSC analysis provided further insights into the crystallinity of the hydrogels (Figures 3A-B), revealing that SEDA-110 hydrogels showcased the highest endothermic peak, indicative of a dry state crystallinity of 46.73%. The crystallization kinetics of PVA are contingent upon the alignment and entanglement of PVA molecular chains, inherently influenced by both annealing temperature and duration. Increased annealing temperature facilitates enhanced molecular mobility and chain entanglement, thereby augmenting the material's crystallinity.[32] This phenomenon elucidates the observed disparity in dry state crystallinity, with SEDA-90 hydrogels manifesting a lower crystallinity of 28.18% compared to their SEDA-110 counterparts. The progression of PVA crystallinity initially enlarges with extended annealing durations, reaching a plateau as the PVA concentration intensifies due to water evaporation. This concentration increase imposes a kinetic barrier, decelerating chain mobility and, consequently, the rate of crystallization. Once fully dehydrated, PVA chain movement halts, preventing further increases in crystallinity. Excessively high temperatures can lead to rapid water evaporation, limiting the crystallization time and reducing crystallinity, as observed in SEDA-130 hydrogels. However, the SEDA-130 hydrogels exhibited the highest wet state crystallinity, attributed to their markedly reduced water content compared to the SEDA-90 and SEDA-110 variants, as evidenced in Figure 3C.

SAXS analysis was employed to examine changes within the crystalline domains, using the Bragg equation to determine the average distance between crystalline domains[33,34]. Initial observations showed that SAXS profile of SE hydrogel exhibited a left-shifted peak (Figure 3C), indicative of minimal interference among adjacent crystalline domains. However, post-dry annealing, a significant shift to the right in the peak position was observed, coupled with an increase in peak intensity as the annealing temperature was elevated from 90°C to 130°C. This shift indicated stronger interactions among crystalline domains, leading to a decrease in the average inter-domain distance from 14.07 nm to 8.44 nm (Figure 3D), reflecting enhanced crosslinking and more robust interactions among crystalline domains.

XRD analysis (Figure S6) further complemented these findings by providing insights into the average size of crystalline domains, the peak domain size observed at 110°C (6.85 nm). Further increase in temperature to 130 °C resulted in a domain size of 6.83 nm, indicating no significant change, aligning with the SAXS data (Figure S7). This demonstrates the critical role of annealing temperature in modulating both the spatial distribution and dimensional attributes of crystalline domains within the hydrogel matrix, thereby enhancing polymer chain interactions and promoting crosslinking. A comparison between the size (*D*) and spacing (*L*) of crystalline domains in SEDA hydrogels and other previously reported PVA hydrogels[24,30,35,36] (Figure 3E & Table S1), reveal that SEDA hydrogels boast substantially larger crystalline domains coupled with notably tighter inter-domain spacing.

The crystalline domain changes were visualized by AFM. As shown in phase diagrams (Figures 3F-I), the original SE hydrogel displayed minimal crystalline features, while the three dry-annealed hydrogels exhibited varying degrees of crystalline domain distribution. The SEDA-90 hydrogel exhibited isolated, bright crystalline domains with some dark amorphous regions. Notably, the SEDA-110 hydrogel showed a prolific distribution of uniformly spaced crystalline domains, suggesting an optimal structural arrangement conducive to superior mechanical properties. In contrast, the SEDA-130 hydrogel, despite its dense crystalline domain distribution, lacked uniformity,

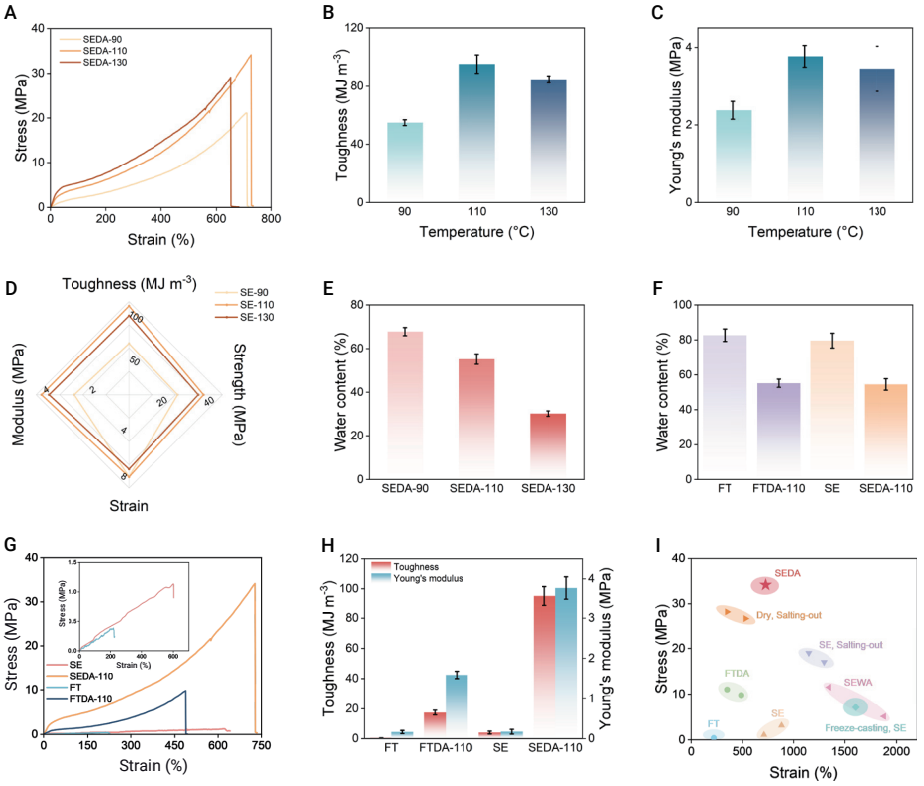

Figure 4. Mechanical characterization of hydrogels (A) Tensile stress–strain curves of different SEDA hydrogels, and (B) the corresponding toughness and (C) Young's modulus. (D) Comparative assessment of mechanical properties among SE, SEDA-90, SEDA-110, and SEDA-130 hydrogels. (E) Water content evaluation for different SEDA hydrogels. (F) Water content of FT, FTDA-110, SE, and SEDA-110 hydrogels. (G) Tensile stress–strain curves of FT, FTDA-110, SE, and SEDA-110 hydrogels and (H) the corresponding toughness and Young's modulus. (I) Comparison of stress versus strain of SEDA-110 hydrogel to previously reported PVA hydrogels.

potentially compromising its mechanical performance.[37]

A comprehensive model was developed to encapsulate the effects of SEDA method on the PVA hydrogel microstructure (Figure 3J). Initially, the solvent-exchanged hydrogel presented a uniform network with limited crystalline domains. The dry annealing process then induced water molecule evaporation, leading to an expansion in both the number and size of crystalline domains, alongside a decrease in the space among adjacent domains. Rehydration transformed this structured matrix into SEDA hydrogels characterized by a dense, evenly distributed, highly crosslinked crystalline network. The average inter-domain distance in the dry state was approximately 6.77 nm, which expanded upon swelling due to polymer chain elongation (Figure S8). This microstructural evolution underscores the effectiveness of SEDA in enhancing the formation and distribution of large crystalline domains, affirming the superior structural integrity and mechanical performance of SEDA hydrogels.

Mechanical properties and structural evolution of SEDA hydrogels

The mechanical properties of SEDA hydrogels, as presented in Figures 4A-D, were thoroughly examined across a range of annealing temperatures from 90°C to 130°C. A notable enhancement in mechanical strength was observed with the transition from SEDA-90 to SEDA-110, evidenced by an increase in the tensile stress from 21.05 MPa to 34.15 MPa and in toughness from 54.88 MJ m^{-3} to 95.21 MJ m^{-3}. However, a further increment to 130°C (SEDA-130) resulted in a decrease in these metrics, with stress reducing to 29.11 MPa and toughness to 84.71 MJ m^{-3}. Contrary to typical hydrogels where mechanical properties increase with decreasing water content, our observations differ. For SEDA hydrogels, the optimal mechanical performance was observed in SEDA-110, which has a water content of 55% (Figure 4E). Although water content declines from 67.8% in SEDA-90 to about 30% in SEDA-130, the SEDA-130 variant exhibited weaker mechanical properties. This unexpected trend can be attributed to the lower wet crystallinity and nonuniform crystalline domain distribution in the SEDA-130 hydrogel, highlighting the critical influence of a dense, uniformly structured polymer network enriched with tightly crosslinked crystalline domains on the hydrogel's mechanical attributes.

The dry annealing process notably reduced the water content in FTDA hydrogels as well (Figure 4F), resulting in diminished hydrogel thickness and enhanced PVA chain entanglement, thereby elevating the mechanical strength of FTDA hydrogels compared to their FT predecessors. This improvement mirrors the enhancements seen in SEDA hydrogels over their SE origins. Despite the precursor process-whether FT or SE-the dry annealing led to hydrogels with comparable water content levels. However, with similar hydration levels, SEDA-110 hydrogels outshone FTDA variants (Figure 4G), achieving an ultimate stress of 34.15 MPa and an ultimate strain of 727.78%, markedly higher than the FTDA-110 hydrogel, which showed an ultimate stress of 9.77 MPa and an ultimate strain of 487.81%. This disparity accentuates the profound impact of network uniformity on mechanical properties prior to dry annealing, as illustrated in Figure 1A.

The SEDA hydrogels also excelled in terms of toughness (95.21 ± 6.26 MJ m^{-3}) and Young's modulus (3.77 ± 0.28 MPa), demonstrating superior deformation resistance (Figure 4H). In contrast, SEWA hydrogels, derived from solvent exchange followed by wet annealing, showcased larger strain capacities (890-997%), indicative of enhanced polymer chain entanglement and crosslinking. However, this process resulted in lower stress levels in SEWA hydrogels (3.92 MPa), toughness (22.48 MJ m^{-3}) and Young's modulus (0.36 MPa), as shown in Figure S9, most likely due to minor changes in network density during the wet annealing process (Figure 1B). The SEDA methodology, characterized by its homogeneous PVA/DMSO solution preparation and controlled anisotropic drying, surpassed the FTDA and SEWA techniques by promoting the formation of extensive, uniform crystalline domains, which significantly contributed to the superior mechanical strength of the hydrogels. Moreover, the mechanical performance of SEDA-110 hydrogels exceeded that of previously reported PVA hydrogels prepared via freeze-thaw or salting-out methods[20,24,36,38] (Table S2, Supporting Information), as shown in Figure 4I. This achievement highlights the effectiveness of the SEDA strategy, underscoring the pivotal role of network uniformity and the distribution of large crystalline domains in defining the mechanical properties of hydrogels.

To rigorously evaluate the stress-relaxation and absorption capabilities of the SEDA-110 hydrogel, its energy dissipation under cyclic stretching-unloading conditions was quantitatively analyzed. During a series of 10 cycles at a fixed strain of 1, as shown in Figures 5A & S10, the SEDA-110 hydrogel exhibited significant hysteresis, indicative of energy loss within the material. The initial cycle revealed a notably high energy dissipation of 1.74 MJ m^{-3}, as illustrated in Figure 5B, suggesting that the deformation predominantly involved the rupture of internal hydrogen bonds. Subsequent cycles displayed relatively consistent energy dissipation levels, implying the hydrogel's internal network structure remained stable despite considerable disruption of hydrogen bonds, thus preventing failure from stress concentration. The Marangoni effect was observed with increasing tensile strain from 1 to 5 during continuous cyclic stretching (Figure 5C), causing a rise in dissipated energy per unit volume from 1.82 MJ m^{-3} to 29.49 MJ m^{-3}, as detailed in Figure 5D. Following the first cycle, the rate of energy dissipation consistently exceeded 72%, highlighting the SEDA-110 hydrogel's ability to effectively

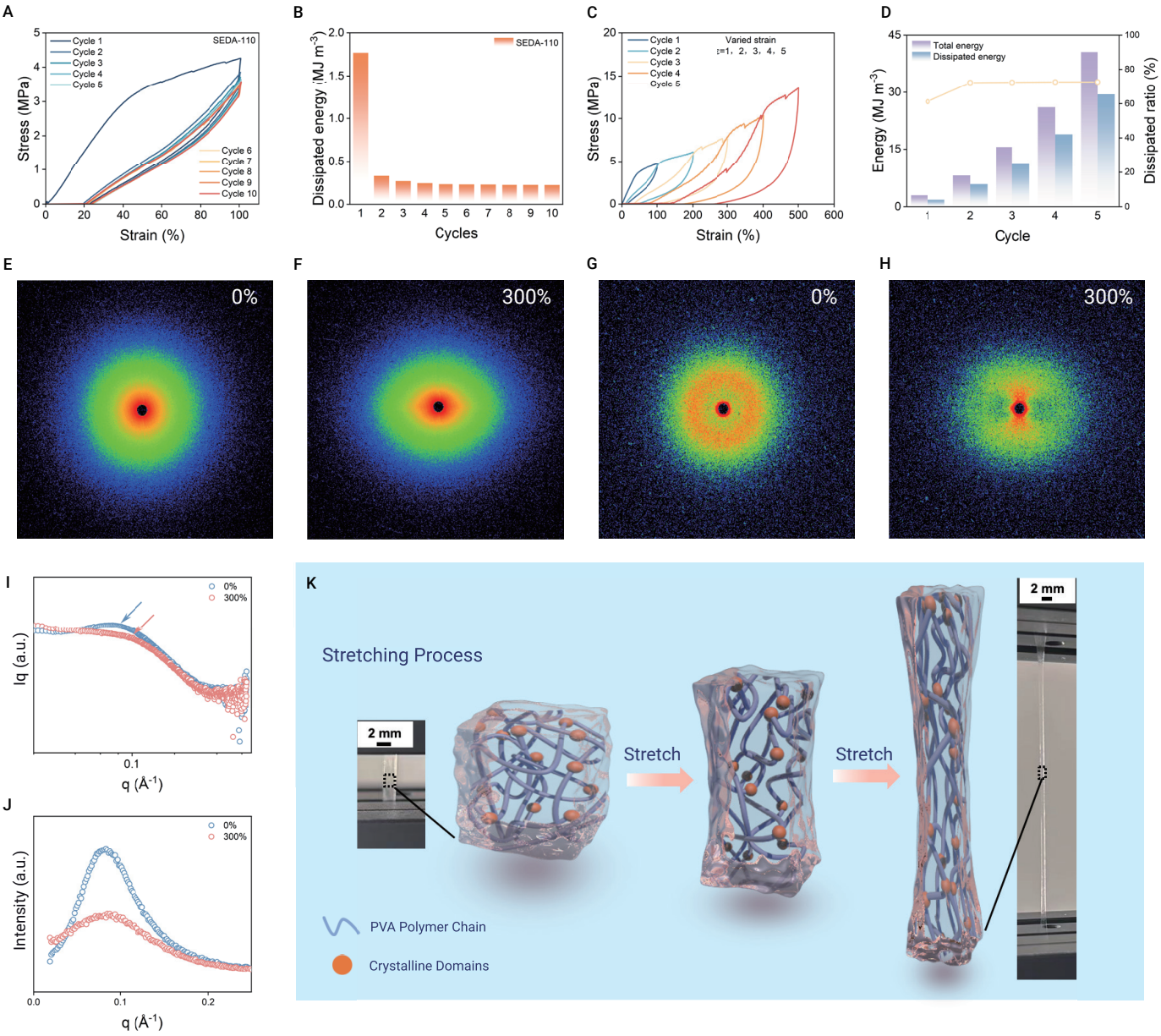

Figure 5. Structural changes of SEDA-110 hydrogel during tensile deformation (A) Cyclic loading-unloading tensile tests of SEDA-110 hydrogel at a strain of 1.0 for 10 cycles, with (B) the corresponding dissipated energy per cycle. (C) Continuous loading-unloading tensile tests under different strains of 1-5 without intervals, and (D) the calculated total energy, dissipated energy, and dissipated ratio. (E-F) SAXS patterns of SE hydrogel during in situ stretching. (G-H) SAXS patterns of SEDA-110 hydrogel during in situ stretching. (I-J) Intensity profiles of SEDA-110 hydrogel during tensile loading. (K) Schematic illustration of the strengthening mechanism.

relieve stress through its homogenous network structure during stretching.

In situ stretching conditions were further investigated using SAXS characterization for both SE and SEDA-110 hydrogels to investigate the mechanism behind the enhancement of hydrogels during stretching. Notably, no significant peaks were detected along the stretching direction for the SE hydrogel over strains from 0% to 300%, as depicted in Figures 5E-F. In contrast, the SEDA-110 hydrogel transitioned from an isotropic to an oriented structure upon stretching, as evidenced in Figures 5G-H & S11, with the average distance between adjacent crystalline domains decreasing from 8 nm to 7.14 nm, as shown in Figures 5I-J. This structural reconfiguration, demonstrated in Figure 5K, suggests that stretching promotes polymer chain alignment in SEDA-110 hydrogel, leading to a more organized and compact polymer network, which in turn enhances the hydrogel's toughness.

Fatigue energy and tunability of SEDA hydrogels

Upon the application of external forces, SEDA hydrogels demonstrate exceptional stress distribution and absorption capabilities due to their dense crystalline domains, effectively hindering crack propagation. The fracture energy, a critical indicator of the hydrogels' resistance to crack growth,[39] was meticulously evaluated using a single-edge notched tensile test (Figure S12). It was found that the fracture energy of the hydrogels varied with the degree of dry annealing; SEDA-90 hydrogel exhibited a fracture energy of 14.27 kJ m^{-2}, SE-110 hydrogel 31.94 kJ m^{-2}, and SEDA-130 hydrogel an impressive 99.2 kJ m^{-2}, as shown in Figure 6A. The inverse relationship between water content and fracture energy post-annealing suggests that the enhanced crystallinity in the SEDA-130 hydrogel contributes to its superior fracture resistance. Compared to other previously reported toughen hydrogels[20,24,36,38,40-43] (Table S3, Supporting Information), SEDA hydrogels stand out for their near-optimal balance of stress resistance, toughness, and fracture energy (Figures 6B-C). A notable demonstration of their mechanical prowess is a SEDA-110 hydrogel sample, measuring 4 cm × 0.5 cm, which successfully lifted an iron pellet weighing approximately 14000 times its own weight (Figure 6D).

Building upon the concept of microstructural densification through salting-

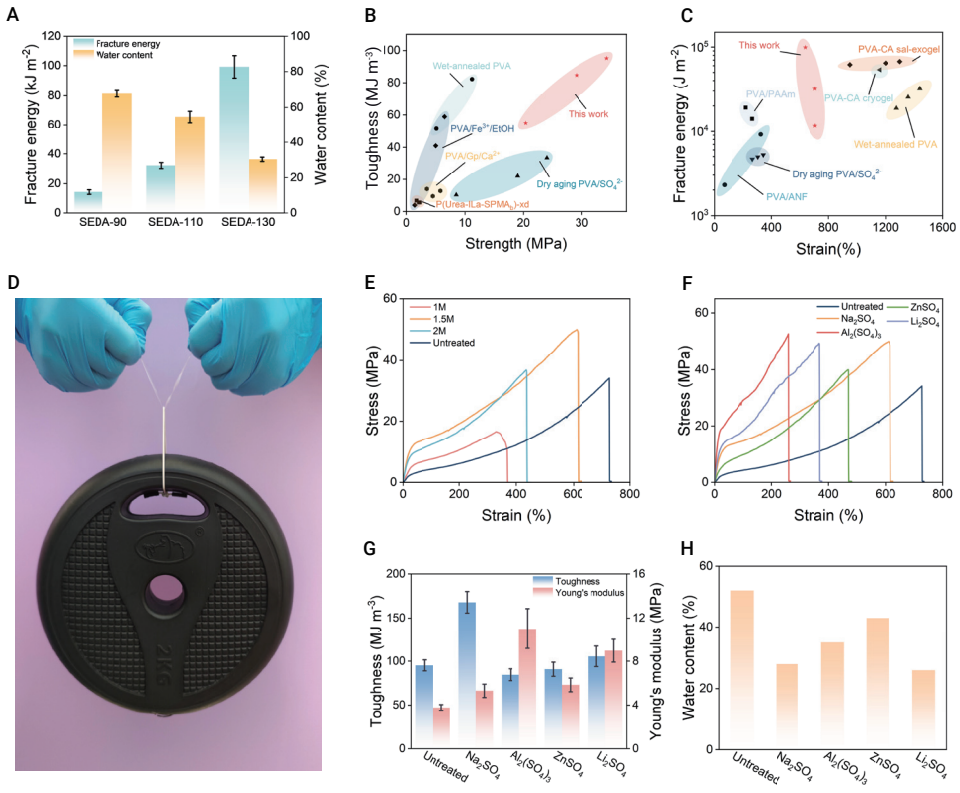

Figure 6. Tunable mechanical properties of PVA Hydrogels produced by SEDA method (A) Fracture energy of different SEDA hydrogels. (B-C) Comparison of toughness versus strength (B), and fracture energy versus strain (C) for SEDA hydrogels in this study versus other reported hydrogels. (D) Photograph of SEDA-110 hydrogel supporting 2 kg, over 12 500× of its own weight. (E) Tensile stress–strain curves of SEDA-110 hydrogel after 48 h of salting out in Na_2SO_4 solutions with various concentrations. (F) Tensile stress–strain curves of SEDA-110 hydrogel after 48 h of salting out in various kosmotropic anions solutions, with (G) corresponding toughness and Young's modulus values, and (H) water content assessment.

out, as pioneered by He et al,[23] we hypothesized that incorporating a salting-out treatment could further enhance the network density of the large crystalline domains for our SEDA hydrogels (Figure S9). To test this, we subjected a SEDA-110 hydrogel to a hypertonic salt solution treatment. This process led to contraction of hydrogel due to the osmotic influx of salt ions and liquid-liquid phase separation, reflecting the aggregation of PVA chains and the formation of new crystalline structures within the matrix. An initial investigation into the effects of various salt solution concentrations revealed that a 1.5 M Na_2SO_4 solution propelled the hydrogel's strain capacity to a peak of 50 MPa, as depicted in Figure 6E. Extending this analysis to other salt solutions while maintaining the same concentration level, it was observed that an $Al_2(SO_4)_3$ solution induced a stress level of 52.5 MPa in the hydrogel, whereas a Na_2SO_4 solution enhanced its toughness to 167.9 MJ m^{-3} (Figures 6F-G). The salting-out process, while enhancing toughness, slightly reduced the hydrogel's strain capacity due to the formation of new crystalline domains that restrict the hydrogel's extensibility under tensile stress. This phenomenon is compounded by the salt-induced entanglement of polymer chains and a reduction in water content, further detailed in Figure 6H. In essence, the strategic integration of the salting-out process with solvent exchange and dry annealing techniques significantly bolsters the mechanical robustness of the SEDA hydrogel, positioning it as a superior contender within the realm of advanced hydrogel systems.

CONCLUSION

In this study, we have unveiled a novel strategy that seamlessly combines solvent exchange with dry annealing to fabricate exceptionally strong and stiff PVA hydrogels. This cutting-edge method allows for the meticulous customization of hydrogel microstructures, ensuring the optimization of polymer network uniformity and crosslinking density as well as the precise regulation of crystalline domain size and distance. Consequently, SEDA hydrogels emerge with a highly organized network, featuring densely packed, large crystalline domains, setting a new benchmark in hydrogel architecture. SEDA hydrogels possess extraordinary mechanical properties, achieving stress levels of 34.15 MPa and toughness of 95.21 MJ m^{-3}, alongside a fracture energy of 99.2 kJ m^{-2}. These figures significantly surpass those of conventional PVA hydrogels fabricated via freeze-thawing and wet annealing techniques. Furthermore, the incorporation of a salting-out process into SEDA hydrogels notably enhances their mechanical properties, pushing strengths up to 52.5 MPa and toughness to 167.9 MJ m^{-3}. Our research demonstrates that the adjustable mechanical properties derived from controlled microstructural evolution, may open up avenues for a revolution in material design, especially in sectors that demand ultra-strong and stiff hydrogels.

REFERENCES

1. Yuk, H., Varela, C.E., Nabzdyk, C.S., et al. (2019). Dry double-sided tape for adhesion of wet tissues and devices. Nature **575**: 169–174. DOI: 10.1038/s41586-019-1710-5.
2. Li, S., Yang, H., Zhu, N., et al. (2023). Biotissue-inspired anisotropic carbon fiber composite hydrogels for logic gates, integrated soft actuators, and sensors with ultra-high sensitivity. Adv. Funct. Mater. **33**: 2211189. DOI: 10.1002/adfm.202211189.
3. Bertsch, P., Diba, M., Mooney, D.J., et al. (2023). Self-healing injectable hydrogels for tissue regeneration. Chem. Rev. **123**: 834–873. DOI: 10.1021/acs.chemrev.2c00179.
4. Sun, X., Pang, Z., Zhu, Y., et al. (2023). All-cellulose hydrogel-based adhesive. The Innovation Materials **1**: 100040. DOI: 10.59717/j.xinn-mater.2023.100040.
5. He, Z., Chen, Y., Li, J., et al. (2024). Hofmeister effect regulated gel iontronic sensor for wide-range pressure perception. The Innovation Materials **2**. DOI: 10.59717/j.xinn-mater.2024.100078.
6. Zhang, Y., Zhang, Y., Deng, J., et al. (2024). In situ electrochemically-bonded self-adapting polymeric interface for durable aqueous zinc ion batteries. Adv. Funct. Mater. **34**: 2310995. DOI: 10.1002/adfm.202310995.
7. Huang, Z., Yang, S., Zhang, Y., et al. (2024). Ultrathin reed membranes: Nature's intimate ion-regulation skins safeguarding zinc metal anodes in aqueous batteries. Adv. Energy Mater. **14**: 2400033. DOI: 10.1002/aenm.202400033.
8. Zeng, Z., Yu, L., Yang, S., et al. (2024). Tuning water-cellulose interactions via copper-coordinated mercerization for hydro-actuated, shape-memory cellulosic hydroplastics. Matter **7**: 3036–3052. DOI: 10.1016/j.matt.2024.04.033.
9. Zhang, Z., Chen, G., Xue, Y., et al. (2023). Fatigue-resistant conducting polymer hydrogels as strain sensor for underwater robotics. Adv. Funct. Mater. **33**: 2305705. DOI: 10.1002/adfm.202305705.
10. Liang, X., Chen, G., Lin, S., et al. (2022). Bioinspired 2d isotropically fatigue-resistant hydrogels. Adv. Mater. **34**: 2107106. DOI: 10.1002/adma.202107106.
11. Zhang, Y.S., and Khademhosseini, A. (2017). Advances in engineering hydrogels. Science **356**: eaaf3627. DOI: 10.1126/science.aaf3627.
12. Ye, Y., Wan, Z., Gunawardane, P.D.S.H., et al. (2024). Ultra-stretchable and environmentally resilient hydrogels via sugaring-out strategy for soft robotics sensing. Adv. Funct. Mater. **34**: 2315184. DOI: 10.1002/adfm.202315184.
13. Cui, W., King, D.R., Huang, Y., et al. (2020). Fiber-reinforced viscoelastomers show extraordinary crack resistance that exceeds metals. Adv. Mater. **32**: 1907180. DOI: 10.1002/adma.201907180.
14. Ni, J., Lin, S., Qin, Z., et al. (2021). Strong fatigue-resistant nanofibrous hydrogels inspired by lobster underbelly. Matter **4**: 1919–1934. DOI: 10.1016/j.matt.2021.03.023.
15. Yang, X., Xu, L., Wang, C., et al. (2023). Reinforcing hydrogel by nonsolvent-quenching-facilitated in situ nanofibrosis. Adv. Mater. **35**: 2303728. DOI: 10.1002/adma.202303728.
16. Li, G., Huang, K., Deng, J., et al. (2022). Highly conducting and stretchable double-network hydrogel for soft bioelectronics. Adv. Mater. **34**: 2200261. DOI: 10.1002/adma.202200261.
17. Zhang, M., Yang, Y., Li, M., et al. (2023). Toughening double-network hydrogels by

polyelectrolytes. Adv. Mater. **35**: 2301551. DOI: 10.1002/adma.202301551.
18. Ji, D., Park, J.M., Oh, M.S., et al. (2022). Superstrong, superstiff, and conductive alginate hydrogels. Nat. Commun. **13**: 3019. DOI: 10.1038/s41467-022-30691-z.
19. Wu, S., Hua, M., Alsaid, Y., et al. (2021). Poly(vinyl alcohol) hydrogels with broad-range tunable mechanical properties via the hofmeister effect. Adv. Mater. **33**: 2007829. DOI: 10.1002/adma.202007829.
20. Wu, Y., Zhang, Y., Wu, H., et al. (2023). Solvent-exchange-assisted wet annealing: A new strategy for superstrong, tough, stretchable, and anti-fatigue hydrogels. Adv. Mater. **35**: 2210624. DOI: 10.1002/adma.202210624.
21. Liang, X., Chen, G., Lin, S., et al. (2021). Anisotropically fatigue-resistant hydrogels. Adv. Mater. **33**: 2102011. DOI: 10.1002/adma.202102011.
22. Sun, X., Mao, Y., Yu, Z., et al. (2024). A biomimetic "salting out – alignment – locking" tactic to design strong and tough hydrogel. Adv. Mater. **36**: 2400084. DOI: 10.1002/adma.202400084.
23. Hua, M., Wu, S., Ma, Y., et al. (2021). Strong tough hydrogels via the synergy of freeze-casting and salting out. Nature **590**: 594–599. DOI: 10.1038/s41586-021-03212-z.
24. Xu, L., Qiao, Y., and Qiu, D. (2023). Coordinatively stiffen and toughen hydrogels with adaptable crystal-domain cross-linking. Adv. Mater. **35**: 2209913. DOI: 10.1002/adma.202209913.
25. Liu, J., Lin, S., Liu, X., et al. (2020). Fatigue-resistant adhesion of hydrogels. Nat. Commun. **11**: 1071. DOI: 10.1038/s41467-020-14871-3.
26. Otsuka, E., and Suzuki, A. (2009). A simple method to obtain a swollen pva gel crosslinked by hydrogen bonds. Appl. Polym. Sci. **114**: 10–16. DOI: 10.1002/app.30546.
27. Otsuka, E., Komiya, S., Sasaki, S., et al. (2012). Effects of preparation temperature on swelling and mechanical properties of pva cast gels. Soft Matter **8**: 8129–8136. DOI: 10.1039/C2SM25513H.
28. Deng, J., Chen, N., Yang, S., et al. (2024). Supercooling-driven homogenization and strengthening of hydrogel networks. ACS Appl. Mater. Interfaces. DOI: 10.1021/acsami.4c11192.
29. Peppas, N.A., and Merrill, E.W. (1976). Poly(vinyl alcohol) hydrogels: Reinforcement of radiation-crosslinked networks by crystallization. J. Appl. Polym. Sci. **14**: 441–457. DOI: 10.1002/pol.1976.170140215.
30. Tang, N., Jiang, Y., Wei, K., et al. (2024). Evolutionary reinforcement of polymer networks: A stepwise-enhanced strategy for ultrarobust eutectogels. Adv. Mater. **36**: 2309576. DOI: 10.1002/adma.202309576.
31. Hou, Y., Chen, C., Liu, K., et al. (2015). Preparation of pva hydrogel with high-transparence and investigations of its transparent mechanism. RSC Adv. **5**: 24023–24030. DOI: 10.1039/C5RA01280E.
32. Cheng, H., Zhao, Y., Wei, X., et al. (2024). Supercooling and solvent depletion-driven poly(vinyl alcohol) film formation mechanism as elucidated by in situ synchrotron radiation x-ray scattering. Macromolecules **57**: 1569–1580. DOI: 10.1021/acs.macromol.3c02640.
33. Zhang, R., Zhang, Q., Ji, Y., et al. (2018). Stretch-induced complexation reaction between poly(vinyl alcohol) and iodine: An in situ synchrotron radiation small- and wide-angle x-ray scattering study. Soft Matter **14**: 2535–2546. DOI: 10.1039/C7SM02155K.
34. Men, Y., Rieger, J., Lindner, P., et al. (2005). Structural changes and chain radius of gyration in cold-drawn polyethylene after annealing: Small- and wide-angle x-ray scattering and small-angle neutron scattering studies. J. Phys. Chem. B **109**: 16650–16657. DOI: 10.1021/jp052723g.
35. Lin, S., Liu, X., Liu, J., et al. (2019). Anti-fatigue-fracture hydrogels. Sci. Adv. **5**: eaau8528. DOI: 10.1126/sciadv.aau8528.
36. Liu, D., Cao, Y., Jiang, P., et al. (2023). Tough, transparent, and slippery pva hydrogel led by syneresis. Small **19**: e2206819. DOI: 10.1002/smll.202206819.
37. Wan, H., Wu, B., Hou, L., et al. (2024). Amphibious polymer materials with high strength and superb toughness in various aquatic and atmospheric environments. Adv. Mater. **36**: 2307290. DOI: 10.1002/adma.202307290.
38. Dong, X., Guo, X., Liu, Q., et al. (2022). Strong and tough conductive organo-hydrogels via freeze-casting assisted solution substitution. Adv. Funct. Mater. **32**: 2203610. DOI: 10.1002/adfm.202203610.
39. Liao, T., Yang, X., Zhao, X., et al. (2021). Gaussian and non-gaussian distributions of fracture properties in tensile stretching of high-density polyethylene. Macromolecules **54**: 8860–8874. DOI: 10.1021/acs.macromol.1c00944.
40. Chen, K., Liang, K., Liu, H., et al. (2023). Skin-inspired ultra-tough supramolecular multifunctional hydrogel electronic skin for human–machine interaction. Nanomicro Lett **15**: 102. DOI: 10.1007/s40820-023-01084-8.
41. Long, T., Li, Y., Fang, X., et al. (2018). Salt-mediated polyampholyte hydrogels with high mechanical strength, excellent self-healing property, and satisfactory electrical conductivity. Adv. Funct. Mater. **28**: 1804416. DOI: 10.1002/adfm.201804416.
42. Xu, L., Zhao, X., Xu, C., et al. (2018). Water-rich biomimetic composites with abiotic self-organizing nanofiber network. Adv. Mater. **30**: 1703343. DOI: 10.1002/adma.201703343.
43. Li, J., Suo, Z., and Vlassak, J.J. (2014). Stiff, strong, and tough hydrogels with good chemical stability. J. Mater. Chem. B **2**: 6708–6713. DOI: 10.1039/C4TB01194E.

FUNDING AND ACKNOWLEDGMENTS

This work was supported by National Natural Science Foundation of China (grant nos. 22461142135 and 22479046). The funders had no role in study design, data collection and analysis, decision to publish or preparation of the manuscript.

AUTHOR CONTRIBUTIONS

Z.W.: conceptualization, supervision, acquired funding, methodology, writing. J. L.: supervision, reviewing article. N.C.: methodology, investigation, validation, formal analysis, data curation, and writing original draft. J.D.: data curation. S.Y.: software. S.X.: data curation. J. S.: software. K.G.: language editing, reviewing.

DECLARATION OF INTERESTS

The authors declare no competing interests.

DATA AND CODE AVAILABILITY

The authors state that the primary data supporting the findings of this study are presented within the paper. Additional data are available upon reasonable request from the corresponding author.

SUPPLEMENTAL INFORMATION

It can be found online at https://doi.org/10.59717/j.xinn-mater.2024.100101

LEAD CONTACT WEBSITE

http://grzy.hnu.edu.cn/site/index/wangchaohui